Passivity-Based Design of a Fractional-Order Virtual Capacitor for Active Damping of Multiparalleled Grid-Connected Current-Source Inverters

M. Ali Azghandi, S. Masoud Barakati, *Senior Member, IEEE*, and Amirnaser Yazdani, *Senior Member, IEEE*

***Abstract*—Current-source inverters (CSIs) have advantages, such as voltage boosting capability and direct current controllability, in high-power conversion applications with low switching frequency. However, inadequate damping of the passive CL filter gives rise to low-order harmonic resonance. The recent research regarding active damping techniques generally focuses on resonance mitigation of single grid-connected inverters. However, multiple resonances that arise from dynamic interactions among paralleled grid-connected inverters compromise system stability and power quality. This article presents the delay-dependent passivity-based analysis and design of a lossless fractional-order virtual capacitor for resonance damping of multiparalleled grid-connected CSI-based systems. Fractional-order capacitors provide a higher degree of freedom that enhances the frequency behavior and robustness of the control. Simulation and experimental results demonstrate the effectiveness of the proposed active damping control even with variations in the grid impedance and the number of paralleled CSIs.**

***Index Terms*—Active damping, current-source inverter (CSI), fractional-order control, parallel converters, virtual capacitor.**

I. Introduction

CURRENT-SOURCE inverters (CSIs) have traditionally been used in high-power variable-speed drives and high-voltage direct current systems due to their voltage boosting capability and direct current controllability. Over the past few years, high-frequency CSIs have also been adopted for renewable energy grid integration and active power filter applications [1]. The CSIs generally operate with low switching frequencies to reduce power losses. However, insufficient damping of the passive CL-filter gives rise to resonated low-order current harmonics from semiconductor switching and degrades the CSI stability [2]. A distorted grid voltage can also worsen the resonance problem and often makes multiple resonant controllers inevitable for selective harmonic compensation in an extended frequency range. The combination of resonance damping control and selective harmonic compensation requires a large stability margin [3].

Manuscript received August 19, 2021; revised December 10, 2021; accepted January 15, 2022. Date of publication February 4, 2022; date of current version March 24, 2022. Recommended for publication by Associate Editor S. A. Khajehoddin. *(Corresponding author: S. Masoud Barakati.)*

M. Ali Azghandi and S. Masoud Barakati are with the University of Sistan and Baluchestan, Zahedan 98167-45845, Iran (e-mail: azghandi@pgs.usb.ac.ir; smbaraka@ece.usb.ac.ir).

Amirnaser Yazdani is with Ryerson University, Toronto, ON M5B 2K3, Canada (e-mail: yazdani@ryerson.ca).

This article has supplementary material provided by the authors and color versions of one or more figures available at https://doi.org/10.1109/TPEL.2022.3148242.

Digital Object Identifier 10.1109/TPEL.2022.3148242

Until now, several active damping techniques have been presented to damp the CL-filter resonance for CSI-based systems. A virtual resistor modifies the dynamic characteristics of the passive filter to damp the harmonics resonance without any increment in the power losses [4]. Depending on the location of the virtual resistor, the active damping consists of voltage feedback from the filter inductor or the filter capacitor [5]. The capacitor voltage feedback introduces a virtual resistor in parallel with the filter capacitor without extra sensors [6]. However, the phase lag associated with computational and modulation delays reshapes the virtual resistor to a virtual impedance [7]. The virtual impedance comprises a resistance that may result in negative damping dependent on the ratio of resonant frequency to sampling frequency [8]. Moreover, grid inductance variations change the resonant frequency of the passive filter [9]. Consequently, the control implementation delays and grid inductance variations cause poor robustness and call for a careful design of active damping. Combined feedback of the capacitor voltage and current emulates a virtual RC damper in parallel with the filter capacitor [10]. However, multiloop active damping reduces system reliability due to extra measurement sensors. As the time derivative of the capacitor voltage corresponds to the capacitor current, proportional–derivative feedback from the only capacitor voltage can adjust both the resonant frequency and the damping ratio of the CL-filter [11]. Since a perfect derivative controller is not implementable due to measurement noise amplification, the derivative term should also include an additional low-pass filter that changes the characteristics of the virtual impedance [12]. The desired digital filter for active damping can also be a lead-lag network, a second-order differential, or a higher order filter [13]. This way, no extra sensor is required, but the filter-based active damping depends on accurate filter tuning.

As technical or economic considerations restrict the rating of switching devices, multiple CSIs can operate in parallel to increase the power rating [14]. The coupling effects among paralleled inverters can excite resonance modes in a cluster of grid-connected CSIs. Furthermore, the equivalent grid inductance seen from paralleled CSIs is larger than that of a single CSI and shifts the resonant frequency toward low frequencies [15]. Multiparalleled grid-connected CSIs require a more elaborate design for their active dampers. However, there is a gap in the published research concerning paralleled CSIs. Thus, few research works have addressed the stability analysis and resonance damping of multiple grid-connected voltage-source inverters (VSIs) [16]–[18].

Fractional-order capacitors are becoming increasingly important due to their higher degree of freedom in controlling

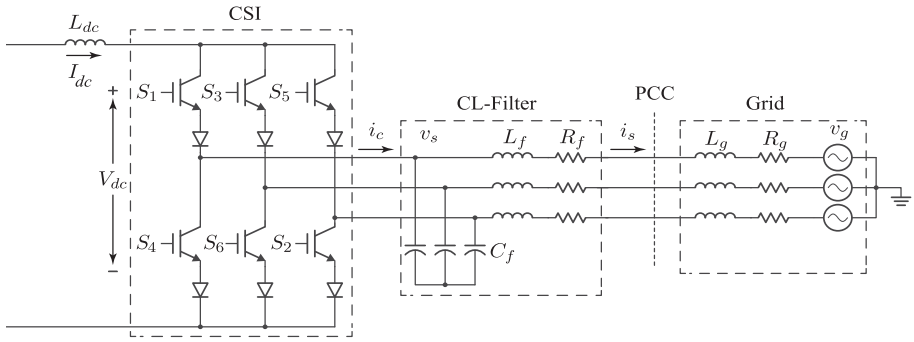

Fig. 1. Schematic diagram of a grid-connected CSI.

the frequency behavior [19]. A fractional-order capacitor generalizes the standard virtual impedance and can consequently offer superior performance. Besides passive RC networks or active emulators, integer-order approximation by rational filters is available to approximate a fractional-order capacitor [20]. The impedance-based analysis approach can be applied to characterize the interaction of grid-connected inverters, and therefore, frequency-domain passivity can be employed to design the virtual impedance [21].

This article proposed a fractional-order virtual capacitor (FOVC) for the active damping of multiparalleled grid-connected CSIs. The FOVC is implemented by capacitor voltage feedback through a fractional-order derivative controller that compensates for the digital control delays. It is worth mentioning that the aliasing distortion and switching noise is almost avoided in the synchronous sampling of the capacitor voltage. The main contributions of this article to the research field are as follows.

1) Although the resonance problems of paralleled VSIs have been reported in several research works, the tools available to analyze the harmonic resonance of paralleled CSIs are tenuous. Hence, the accurate impedance-based model for multiparalleled grid-connected CSIs is established via Norton's equivalent circuits.
2) The passivity-based approaches that have been recently applied to converter damping design need more attention to ensure an adequate stability margin for parallel CSIs. For this purpose, a straightforward tuning method is used to carefully design the multiresonance active damper considering the digital control delays.
3) From the robust control point of view, a fractional-order controller is advantageous due to its adjustable noninteger differentiator order and reduces sensitivity to high-frequency noise compared to a perfect derivative. The proposed FOVC as a generalized virtual impedance has a superior performance with an extended active damping region compared with the existing filter-based active damping methods without additional sensors.

The rest of this article is organized as follows. First, the impedance-based model of multiparalleled grid-connected CSIs is established. Then, frequency-domain passivity-based design and digital approximation of the proposed FOVC are presented. Finally, simulation and experimental results confirm that the proposed FOVC as a combination of RC dampers efficiently mitigates the CL-filter resonance even with variations in the grid impedance and the number of paralleled CSIs.

II. System Modeling and Control

Fig. 1 shows a simplified schematic diagram of a three-phase grid-connected CSI with a passive CL-filter. In balanced three-phase systems, the relationships between the space-phasor and dq-frame time-invariant variables are given by

$$\overrightarrow{x}(t) = (X_d + jX_q)\, e^{j\delta} \tag{1}$$

$$\frac{d\overrightarrow{x}(t)}{dt} = \left(\left(\frac{dX_d}{dt} - \omega X_q \right) + j \left(\frac{dX_q}{dt} + \omega X_d \right) \right) e^{j\delta} \tag{2}$$

where $\overrightarrow{x}$ represents a space phasor variable, X_d and X_q are the equivalent dq-frame components, δ is the reference angle of the dq frame, and $\omega = d\delta/dt$ denotes the dq-frame angular speed.

A state-space model of the grid-connected CSI in the synchronous reference frame can be described by

$$\frac{dV_{sd}}{dt} = \frac{1}{C_f}(I_d - I_{sd}) + \omega V_{sq} \tag{3}$$

$$\frac{dV_{sq}}{dt} = \frac{1}{C_f}(I_q - I_{sq}) - \omega V_{sd} \tag{4}$$

$$\frac{dI_{sd}}{dt} = \frac{1}{L_{\text{ac}}}(V_{sd} - V_d - R_{\text{ac}} I_{sd}) + \omega I_{sq} \tag{5}$$

$$\frac{dI_{sq}}{dt} = \frac{1}{L_{\text{ac}}}(V_{sq} - V_q - R_{\text{ac}} I_{sq}) - \omega I_{sd} \tag{6}$$

where (V_{sd}, V_{sq}), (I_{sd}, I_{sq}), (I_d, I_q), and (V_d, V_q) signify the dq components of the filter capacitor voltage v_s, the filter inductor current i_s, the CSI output current i_c, and the grid voltage v_g, respectively. Furthermore, $R_{\text{ac}} = R_f + R_g$ and $L_{\text{ac}} = L_f + L_g$ are the total series resistance and inductance of the filter inductor and the host grid.

The control strategy of the grid-connected CSI-based system consists of the dc-side current loop cascaded with the ac-side current loop. It is advisable to design the ac-side current control with a time constant in the range of five to ten times the sampling period and a percentage overshoot of less than 5% for a fast and accurate response. Generally, the design of the dc-side current controller aims at achieving five to ten times slower dynamics than the ac-side current to decouple the cascaded control loops. The ac-side current loop is responsible for power quality and is, therefore, affected by active damping control. The dc-side current is also regulated as constant by a proportional–integral (PI) controller.

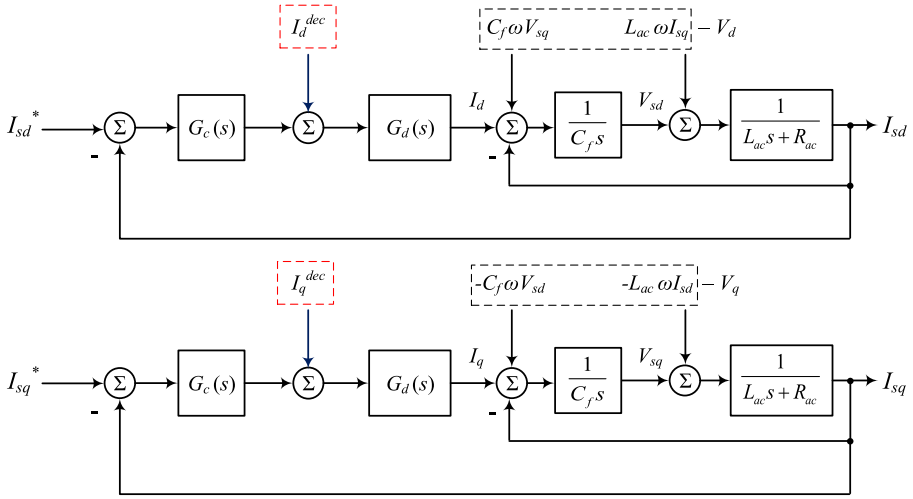

Fig. 2. Control structure for the ac-side current.

Fig. 2 shows the ac-side current control loops based on (3)–(6) implementing the PI controller $G_c(s)$. The active current reference, I_{sd}^*, is determined based on the desired output power throughput at the point of common coupling (PCC), whereas the reactive current reference, I_{sq}^*, is set to zero for unity power factor operation. The transfer function for the digital delays arising from computation and pulsewidth modulation (PWM) can be approximated in terms of the sampling period, T_s, as [22]

$$G_d(s) = e^{-1.5T_s s}. \tag{7}$$

The couplings due to the rotating reference frame transformation can be eliminated by the following decoupling signals:

$$I_d^{\text{dec}} = -C_f\omega V_{sq} - C_f L_{\text{ac}}\omega \frac{dI_{sq}}{dt} \tag{8}$$

$$I_q^{\text{dec}} = C_f\omega V_{sd} + C_f L_{\text{ac}}\omega \frac{dI_{sd}}{dt}. \tag{9}$$

Considering a PI controller with the proportional gain K_p and the integral gain K_i, the closed-loop transfer function of the ac-side current without time delays can be determined as follows:

$$\frac{I_{sd}}{I_{sd}^*} = \frac{I_{sq}}{I_{sq}^*} = \frac{\frac{K_i}{L_{\text{ac}}C_f}\left(\frac{K_p}{K_i}s+1\right)}{s^3 + \frac{R_{\text{ac}}}{L_{\text{ac}}}s^2 + \frac{1+K_p}{L_{\text{ac}}C_f}s + \frac{K_i}{L_{\text{ac}}C_f}}. \tag{10}$$

By the Routh–Hurwitz stability criterion, the stability of the system requires

$$K_i < \frac{R_{\text{ac}}}{L_{\text{ac}}}(1+K_p). \tag{11}$$

It is evident that negligible passive resistance results in a narrow stability region.

The transfer functions of the ac-side current to the system harmonics from the PWM process and the grid voltage distortions are given by

$$G_{ii}(s) = \frac{I_{sd}}{I_d} = \frac{I_{sq}}{I_q} = \frac{1}{s^2 L_{\text{ac}}C_f + sR_{\text{ac}}C_f + 1} \tag{12}$$

$$G_{iv}(s) = \frac{I_{sd}}{V_d} = \frac{I_{sq}}{V_q} = \frac{-sC_f}{s^2 L_{\text{ac}}C_f + sR_{\text{ac}}C_f + 1}. \tag{13}$$

The damping ratio ζ, the natural frequency ω_n, and the resonant frequency ω_r of the passive CL-filter are

$$\zeta = \frac{R_{\text{ac}}}{2}\sqrt{\frac{C_f}{L_{\text{ac}}}} \tag{14}$$

$$\omega_n = \frac{1}{\sqrt{L_{\text{ac}}C_f}} \tag{15}$$

$$\omega_r = \omega_n\sqrt{1-2\zeta^2}. \tag{16}$$

The magnitude of the ac-side current response at the natural frequency is then given by

$$\left|G_{ii}(j\omega_n)\right| = \frac{1}{2\zeta} \tag{17}$$

$$\left|G_{iv}(j\omega_n)\right| = \frac{C_f\omega_n}{2\zeta}. \tag{18}$$

As can be seen, with insufficient damping, the CL-filter resonance magnifies the current harmonics caused by the CSI current or the grid voltage.

III. Multiparallel Grid-Connected CSIs

Commonly, CSIs operate in parallel to scale up the current injected into the grid. Hence, dynamic interactions between the paralleled CSIs and the host grid further affect the system stability and power quality. Fig. 3 shows the circuit model and its Norton equivalent for a system of N paralleled CSIs connected to the host grid through passive CL-filters. The Norton current and admittance in Fig. 3 are calculated as follows:

$$G_{ck}(s)i_{ck} = \frac{1}{s^2 L_{fk}C_{fk} + sR_{fk}C_{fk} + 1}i_{ck} \tag{19}$$

$$Y_{fk}(s) = \frac{sC_{fk}}{s^2 L_{fk}C_{fk} + sR_{fk}C_{fk} + 1}. \tag{20}$$

The current injected into the grid by Inverter 1 is given by

$$i_{s1} = G_{1,1}(s)i_{c1} + \sum_{k=2}^{N} G_{k,1}(s)i_{ck} + G_{v,1}(s)v_g \tag{21}$$

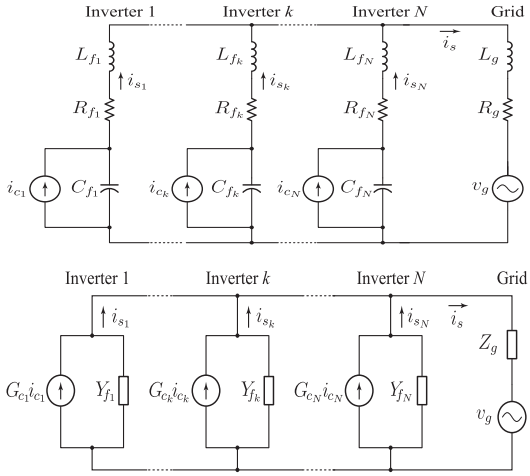

Fig. 3. Circuit model (top) and Norton equivalent (bottom) of multiparalleled grid-connected CSIs.

where

$$G_{1,1}(s) = \left(1 - \frac{Z_g(s)Y_{f1}(s)}{1 + Z_g(s)\sum_{k=1}^{N} Y_{fk}(s)}\right) G_{c1}(s) \quad (22)$$

$$G_{k,1}(s) = \left(\frac{-Z_g(s)Y_{f1}(s)}{1 + Z_g(s)\sum_{k=1}^{N} Y_{fk}(s)}\right) G_{ck}(s) \quad (23)$$

$$G_{v,1}(s) = \frac{-Y_{f1}(s)}{1 + Z_g(s)\sum_{k=1}^{N} Y_{fk}(s)}. \quad (24)$$

As can be seen from (21)–(24), multiparalleled grid-connected CSIs have three different resonant modes: 1) internal resonance due to the self-current harmonics of each CSI; 2) parallel resonance due to the mutual-current harmonics of the other CSIs; and 3) series resonance due to the voltage harmonics of the host grid. As the number of paralleled CSIs increases, the equivalent parallel admittance seen from the single CSI becomes larger. Meanwhile, the CSIs get decoupled from each other if the grid impedance is zero.

Fig. 4 illustrates the frequency response of the current injected into the grid by Inverter 1 for various numbers of identical paralleled CSIs. Fig. 4(a) and (b) indicates that the current harmonics of the paralleled CSIs excite two resonance modes, one at a fixed high frequency and the other at a variable low frequency dependent on the number of paralleled CSIs. Fig. 4(c) illustrates that the voltage harmonics of the grid source only excites the low-frequency resonance. The peak amplitude of the low-frequency resonance attenuates with the increased number of parallel CSIs.

If the CL-filter parameters are the same for all CSIs, two natural frequencies of the paralleled CSIs can be further simplified to

$$\omega_{n,h} = \frac{1}{\sqrt{L_f C_f}} \quad (25)$$

$$\omega_{n,l} = \frac{1}{\sqrt{(L_f + NL_g)\,C_f}}. \quad (26)$$

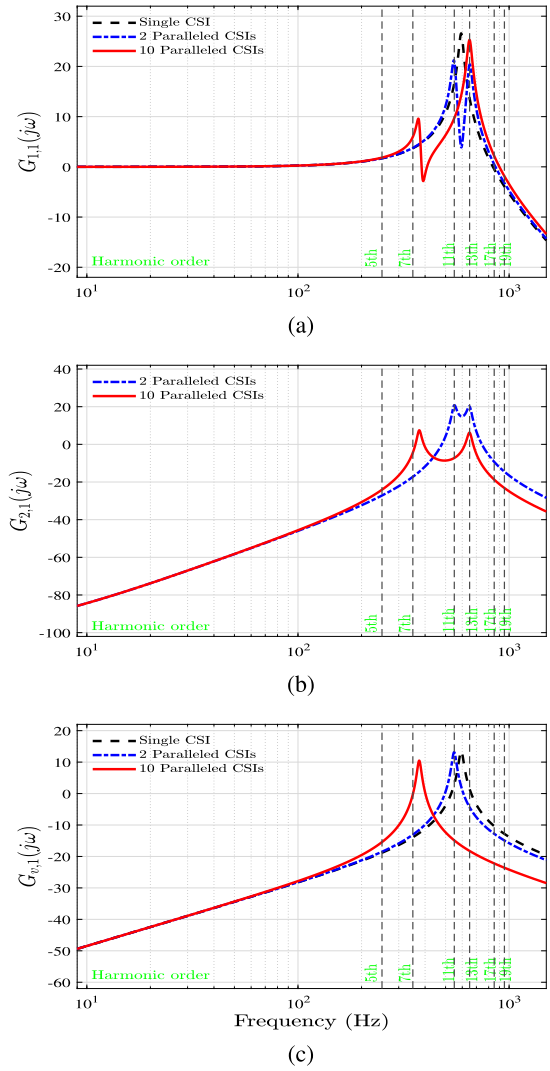

Fig. 4. Frequency response of the current injected into the grid by Inverter 1. (a) Frequency response of $G_{1,1}(j\omega)$. (b) Frequency response of $G_{2,1}(j\omega)$. (c) Frequency response of $G_{v,1}(j\omega)$.

The current injected into the grid by N paralleled CSIs can also be determined as

$$i_s = \frac{1}{1 + Z_g(s)\sum_{k=1}^{N} Y_{fk}(s)}\left(\sum_{k=1}^{N} G_{ck}(s)i_{ck} - \sum_{k=1}^{N} Y_{fk}(s)v_g\right). \quad (27)$$

For identical paralleled CSIs ($i_{ck} = i_c$ and $Y_{fk} = Y_f$), one can write

$$G_{ii}(s) = \frac{1}{s^2\,(L_f + NL_g)\,C_f + (R_f + NR_g)\,C_f + 1} \quad (28)$$

$$G_{iv}(s) = \frac{-sC_f}{s^2\,(L_f + NL_g)\,C_f + (R_f + NR_g)\,C_f + 1}. \quad (29)$$

As can be seen, the equivalent grid impedance is N times larger due to the coupling effect of paralleled CSIs. Hence, the power quality and stability problems for multiparalleled CSIs will become more severe in a weak grid.

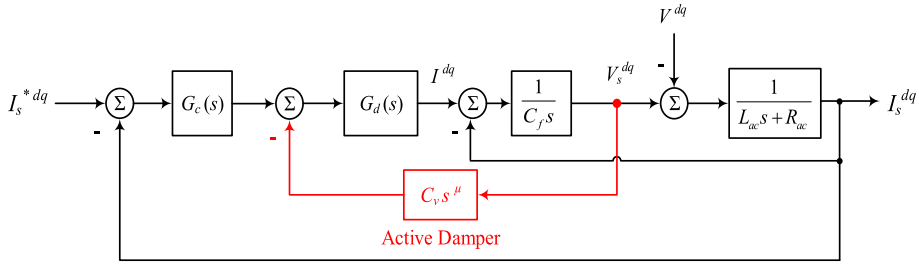

Fig. 5. Control structure for the ac-side current with the proposed active damping loops.

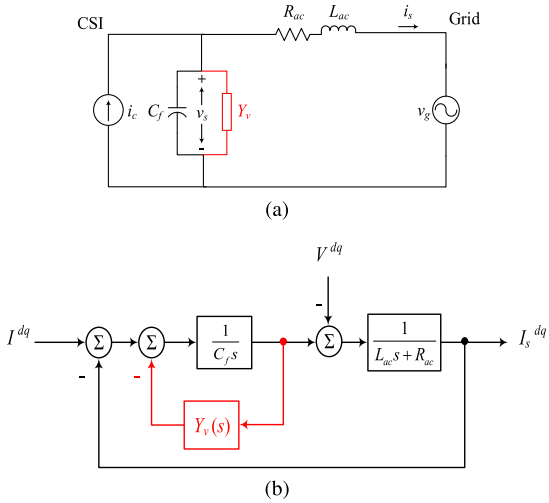

Fig. 6. Equivalent representation of the modified CL-filter with the FOVC. (a) Equivalent circuit. (b) Block diagram representation with delays considered.

IV. Proposed FOVC

The active damping techniques can modify the control algorithm to suppress the harmonic resonance. For a fast and accurate response, both the damping ratio and the resonant frequency of the CL-filter should be adjusted. To that end, this article proposes an FOVC of the form $C_v s^{\mu}$, where the real number μ is the order of differentiation. The capacitor voltage feedback through a fractional-order derivative controller to the PWM reference emulates the proposed FOVC in parallel with the filter capacitor.

Fig. 5 shows the ac-side current control loops for the modified CL-filter with the proposed FOVC. To better understand the illustrated active damping, the ac-side current control with the proposed feedback loop is represented in Fig. 6. Fig. 6(a) and (b) redraws the equivalent circuit and the block diagram of the modified CL-filter with the proposed FOVC. Taking into account the time delays in the control loop, the virtual admittance appearing in parallel with the filter capacitor is

$$Y_v(s) = C_v e^{-1.5T_s s} s^{\mu}. \tag{30}$$

A. Passivity-Based Design

The impedance-based model formed on the Nyquist stability criterion can be applied to analyze the stability of grid-connected CSIs [23]. Impedance-based stability analysis defines the loop gain as the product of the admittance $Y_p(s)$ in parallel with the converter and the impedance $Z_s(s)$ in series with the grid, as shown in Fig. 7. With the active damping loop, the current injected into the grid by N identical paralleled CSIs can be

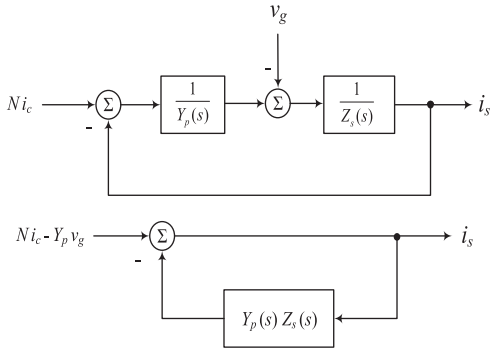

Fig. 7. Basic principle of the impedance-based stability analysis method.

obtained as

$$i_s = \frac{1}{1+Y_p(s)Z_s(s)} Ni_c + \frac{-Y_p(s)}{1+Y_p(s)Z_s(s)} v_g \tag{31}$$

where applying the proposed FOVC leads to

$$Y_p(s) = sC_f + Y_v(s) \tag{32}$$

$$Z_s(s) = s\left(L_f + NL_g\right) + \left(R_f + NR_g\right). \tag{33}$$

The passivity concept presents a sufficient, yet not necessary, stability condition for the modified CL-filter [24]. Since $Z_s(s)$ is passive, the passivity of the desired filter will depend on the real part of $Y_p(s)$. The passive virtual admittance with a positive real part can provide satisfactory resonance damping, which implies that the phase angle of $Y_p(j\omega)$ is within $[-90°, 90°]$. The real and imaginary terms of $Y_v(j\omega)$ are given by

$$\Re[Y_v(j\omega)] = C_v \omega^{\mu} \cos\left(\mu\frac{\pi}{2} - 1.5T_s\omega\right) \tag{34}$$

$$\Im[Y_v(j\omega)] = C_v \omega^{\mu} \sin\left(\mu\frac{\pi}{2} - 1.5T_s\omega\right). \tag{35}$$

The critical frequency ω_v above which the real part of $Y_v(j\omega)$ becomes negative is related to the sampling frequency ω_s as

$$\frac{\omega_v}{\omega_s} = \frac{1}{6}(1+\mu). \tag{36}$$

The resonant frequency of the CL-filter should be below ω_v to ensure a positive phase margin for active damping control. As a result, resonance damping of the N paralleled CSIs calls for

$$\omega_{n,h} = \sqrt{\left(1+\frac{NL_g}{L_f}\right)}\omega_{n,l} < \frac{\omega_s}{6}(1+\mu). \tag{37}$$

The digital control delay affects the critical frequency and narrows the active damping region. For proportional capacitor

voltage feedback ($\mu = 0$), ω_v is equal to one-sixth of the sampling frequency. As seen from (37), the FOVC compensates for the phase lag caused by digital control that promises a smaller passive filter with a higher resonant frequency. The improvement is not limitless so that the active damping region saturates around $\omega_s/3$, corresponding to purely derivative feedback ($\mu = 1$).

Assuming $R_{\text{ac}} = 0$ as the worst damping condition, the passivity-based design of the proposed FOVC involves the following considerations.

1) The desired natural frequency, ω_n^*, should satisfy the following equation:

$$\Im[Y_p(j\omega_n^*)]\Im[Z_s(j\omega_n^*)] = 1. \tag{38}$$

2) The desired damping ratio, ζ^*, should satisfy the following equation:

$$\zeta^* = \frac{1}{2}\Re[Y_p(j\omega_n^*)]\Im[Z_s(j\omega_n^*)]. \tag{39}$$

Therefore, the FOVC parameters can be determined as

$$\mu = \frac{2}{\pi}\left[\tan^{-1}\left(\frac{1-(L_f+NL_g)\,C_f\omega_n^{*2}}{2\zeta^*}\right) + 1.5T_s\omega_n^*\right] \tag{40}$$

$$C_v = \frac{\sqrt{\left(1-(L_f+NL_g)\,C_f\omega_n^{*2}\right)^2 + 4\zeta^{*2}}}{(L_f+NL_g)\,\omega_n^{*(1+\mu)}}. \tag{41}$$

B. Approximation and Realization

There are several definitions for the fractional-order derivative first introduced by Riemann–Liouville and Grunwald. The most common way to realize the fractional differential operator is an approximation by a rational finite-order transfer function. These approximations are valid over a given bandwidth corresponding to the order of approximation. Oustaloup recursive filter approximation is widely used for the implementation of fractional-order controllers. The modified Oustaloup filter approximation is of the form [25]

$$s^{\mu} \approx \left(\frac{\omega_h}{\omega_b}\right)^{-\mu/2} \prod_{k=-n}^{k=n} \frac{\omega_k}{\omega'_k} \prod_{k=-n}^{k=n} \frac{s+\omega'_k}{s+\omega_k} \tag{42}$$

$$\omega_k = \omega_b\left(\frac{\omega_h}{\omega_b}\right)^{\frac{k+n+0.5(1+\mu)}{2n+1}} \tag{43}$$

$$\omega'_k = \omega_b\left(\frac{\omega_h}{\omega_b}\right)^{\frac{k+n+0.5(1-\mu)}{2n+1}} \tag{44}$$

where $2n+1$ is the order of the rational transfer function over the frequency range $\omega_b < \omega < \omega_h$. Meanwhile, a fractional-order capacitor can be approximated based on specific types of passive RC networks or active emulators. Fig. 8 shows a typical RC ladder for emulating a fractional-order capacitor.

Fig. 9 illustrates the impact of the FOVC on the frequency response of the CL-filter for single grid-connected CSI. As shown in Fig. 9(a) and (b), the proposed FOVC efficiently shaves off the filter peak at the resonant frequency. The frequency response of the CL-filter further improves with higher order approximations of the proposed FOVC so that the third-order approximation is satisfactory for resonance damping. Fig. 10

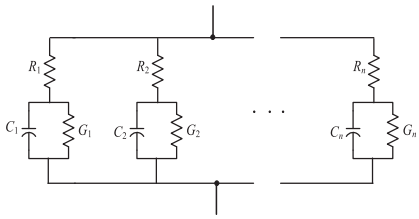

Fig. 8. Passive RC ladder for emulating a fractional-order capacitor.

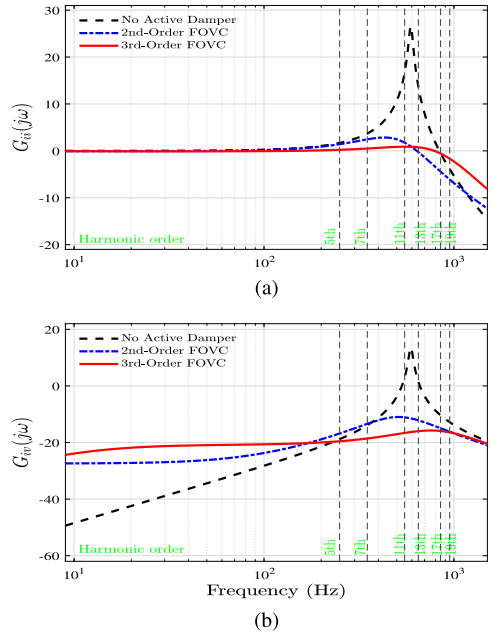

Fig. 9. Frequency response of the CL-filter for single CSI. (a) Frequency response of $G_{ii}(j\omega)$. (b) Frequency response of $G_{iv}(j\omega)$.

shows the frequency response of the current injected into the grid by Inverter 1 for ten identical paralleled CSIs with the active damping control. The proposed FOVC for only Inverter 1 mitigates the internal resonance, as seen in Fig. 10(a). However, the FOVCs of the other CSIs are further required to effectively damp the parallel and series resonances, as shown in Fig. 10(b) and (c).

V. Evaluation Results

To validate the theoretical analysis and to evaluate the performance of the proposed FOVC, the grid-connected CSI-based system is modeled in the MATLAB/Simulink environment. An experimental setup, shown in Fig. 11, is also implemented to validate the simulation results. A TMS320F2812 digital signal processor utilizes measured parameters to realize the designed current control and active damping loops. The circuit and control parameters of the CSI-based system are presented in Table I.

A. Simulation Results

The simulation cases are presented to evaluate the system performance for different numbers of paralleled CSIs. In these cases, a constant current source is considered on the dc side. Fig. 12 shows the simulated waveforms of the current injected into the grid for a single grid-connected CSI. The reference of ac-side current changes from 200 to 250 A at $t = 0.25$ s. Fig. 12(a) and (b) indicates that the proposed FOVC adequately

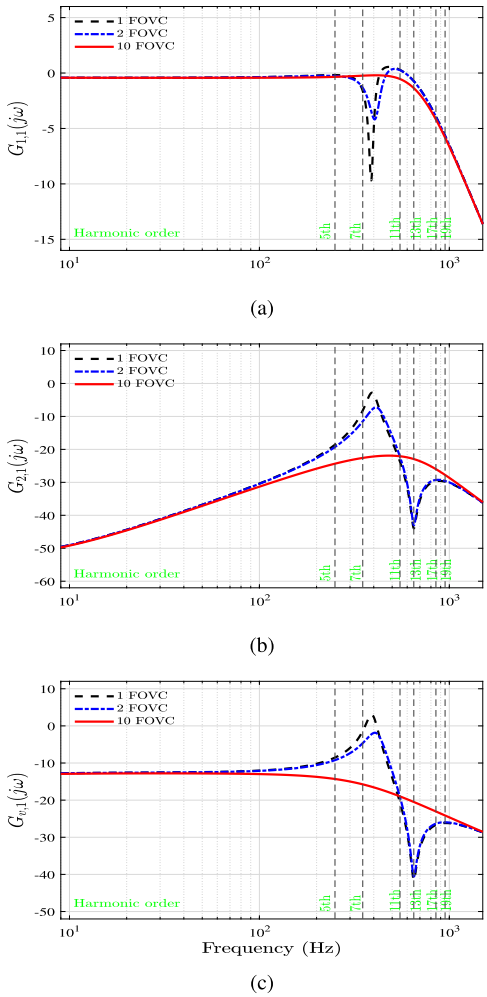

Fig. 10. Frequency response of the current injected into the grid by Inverter 1 for ten paralleled CSIs. (a) Frequency response of $G_{1,1}(j\omega)$. (b) Frequency response of $G_{2,1}(j\omega)$. (c) Frequency response of $G_{v,1}(j\omega)$.

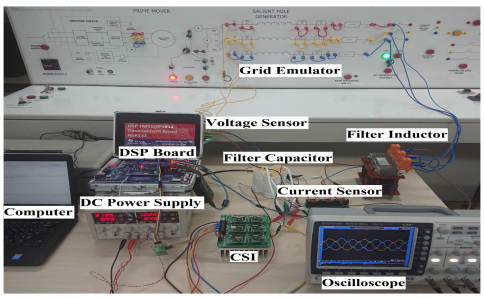

Fig. 11. Hardware prototype setup.

mitigates the current oscillations. Table II lists the low-order current harmonics of the single grid-connected CSI. It is evident that the proposed FOVC effectively attenuates the low-order harmonics.

Fig. 13 shows the simulated waveforms of the current injected into the grid for a set of ten paralleled grid-connected CSIs. The reference of ac-side current for paralleled CSIs is different from each other. The parallel operation of CSIs may also excite the low-order current harmonics. The active damping control is activated at $t = 0.1$ s for Inverter 1 followed by the other CSIs after 0.1 s. Fig. 13(a) illustrates that the current injected into the grid

TABLE I
PARAMETERS OF THE GRID-CONNECTED CSI-BASED SYSTEM

Symbol	Parameter	Simulation	Experiment
V_g	Grid voltage	380 V	190 V
f	Grid frequency	50 Hz	50 Hz
L_g	Grid inductance	0.25 mH	0.25 mH
R_g	Grid resistance	0.01 Ω	0.01 Ω
C_f	Filter capacitor	60 μF	60 μF
L_f	Filter inductor	1 mH	1 mH
R_f	Filter resistor	0.25 Ω	0.25 Ω
f_{sw}	Switching frequency	2500 Hz	2500 Hz
T_s	Sampling period	200 μs	200 μs
K_i	PI integral-gain	500	500
C_v	FOVC pseudo-capacitance	10^{-4}	10^{-4}
μ	FOVC differentiation-order	0.38	0.38

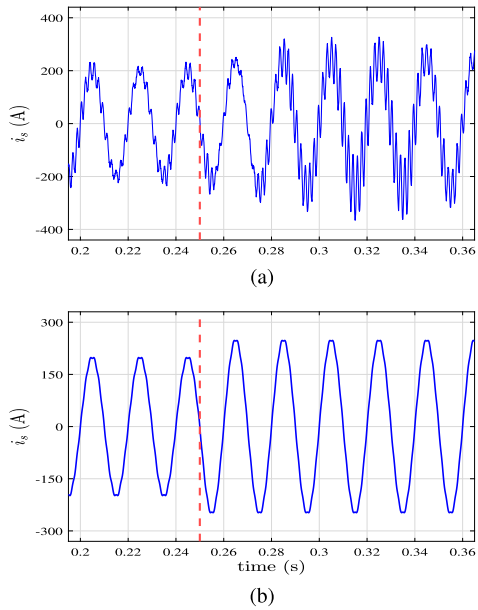

Fig. 12. Simulated current injected into the grid for a single grid-connected CSI. (a) No active damper. (b) With proposed FOVC.

TABLE II
AMPLITUDE OF THE LOW-ORDER CURRENT HARMONICS FOR A SINGLE GRID-CONNECTED CSI

i_s	5th	7th	11th	13th	17th	19th
No active damper	1%	2%	40%	4%	1%	0.5%
Proposed FOVC	0.3%	0.4%	1%	0.5%	0.4%	0.2%

There are still some distortions after activation of the FOVC for Inverter 1. However, the FOVC for all CSIs sufficiently mitigates the current oscillations of Inverter 1. Fig. 13(b) indicates that the total current injected into the grid by ten paralleled CSIs is of better quality due to mitigation of high-frequency resonance, and the FOVC of Inverter 1 effectively suppresses the current oscillations. Table III lists the low-order current harmonics for the set of ten paralleled grid-connected CSIs. As seen, only one FOVC can attenuate the low-order harmonics of the current injected into the grid by multiple CSIs. However, various FOVCs are required to attenuate the current injected into the grid by Inverter 1.

A simulation case is further designed to compare the performance of the proposed FOVC with similar approaches. Fig. 14

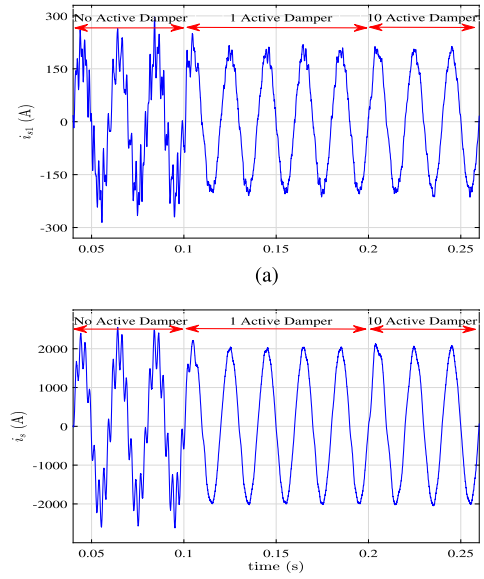

Fig. 13. Simulated current injected into the grid for a set of ten paralleled grid-connected CSIs. (a) Waveform of i_{s1}. (b) Waveform of i_s.

TABLE III
AMPLITUDE OF THE LOW-ORDER CURRENT HARMONICS FOR A SET OF TEN PARALLELED GRID-CONNECTED CSIS

i_{s1}	5th	7th	11th	13th	17th	19th
No active damper	2%	5%	3%	30%	2%	1%
CSI-1 FOVC	1%	3%	2%	10%	1.5%	0.5%
10-CSIs FOVC	0.5%	2%	1%	1.5%	1%	0.5%
i_s	5th	7th	11th	13th	17th	19th
No active damper	1%	25%	1%	3%	2%	1%
CSI-1 FOVC	0.5%	3%	0.5%	1%	0.5%	0.5%
10-CSIs FOVC	0.5%	1.5%	0.2%	1%	0.5%	0.2%

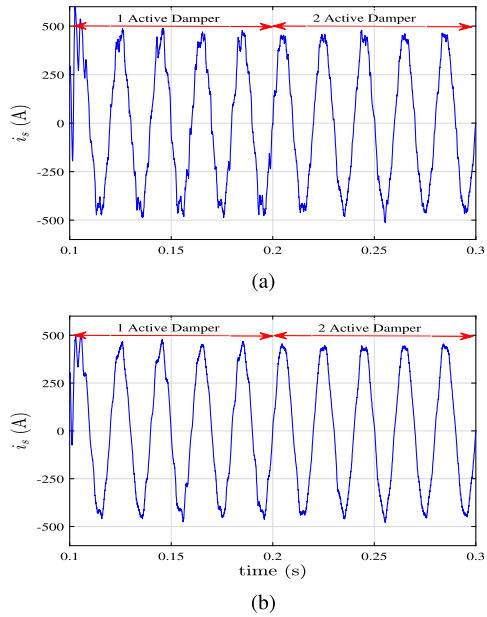

Fig. 14. Simulated current injected into the grid for two paralleled grid-connected CSIs. (a) Second-order FOVC. (b) Third-order FOVC.

TABLE IV
AMPLITUDE OF THE LOW-ORDER CURRENT HARMONICS FOR TWO PARALLELED GRID-CONNECTED CSIS

i_s	5th	7th	11th	13th	17th	19th
CSI-1 Second order FOVC	0.5%	2%	10%	3%	1%	0.5%
CSI-1 Third order FOVC	0.3%	0.5%	4%	1%	0.4%	0.2%
2-CSIs Second order FOVC	0.4%	1%	6%	2%	1%	0.5%
2-CSIs Third order FOVC	0.2%	0.3%	2%	0.5%	0.4%	0.2%

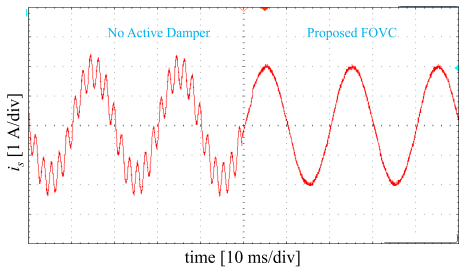

Fig. 15. Measured current injected into the grid for $L_{\text{ac}} = 1.25$ mH.

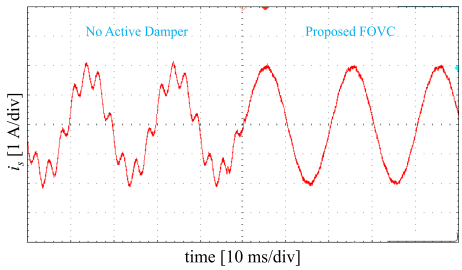

Fig. 16. Measured current injected into the grid for $L_{\text{ac}} = 3.5$ mH.

the grid for two paralleled grid-connected CSIs. The waveform illustrated in Fig. 14(a) corresponds to a second-order approximation of the proposed FOVC. On the other hand, the waveform represented in Fig. 14(b) shows the performance of the third-order FOVC. The second-order FOVC can be considered as an approximation of the second-order filter [2] or the lead-lag network [12] for active damping, which is designed based on passivity characteristics. As a result, the third-order FOVC has a superior damping characteristic against the second-order FOVC. Table IV lists the low-order current harmonics for two paralleled grid-connected CSIs. It can be seen that the third-order FOVC suppresses the current harmonics more effectively than that of the second-order FOVC.

B. Experimental Results

The experimental results are provided to emulate a single grid-connected CSI in a weak grid. A power supply in the constant current mode was implemented to regulate the dc-side current. When the ac-side inductance increases from $L_f + Lg$ to $L_f + 10L_g$, corresponding to ten paralleled CSIs, the resonant frequency decreases from about 11th harmonic to about seventh harmonic. Fig. 15 shows the measured waveforms of the current injected into the grid for $L_{\text{ac}} = 1.25$ mH that verify the simulation results for the efficacy of the proposed FOVC. Fig. 16 illustrates

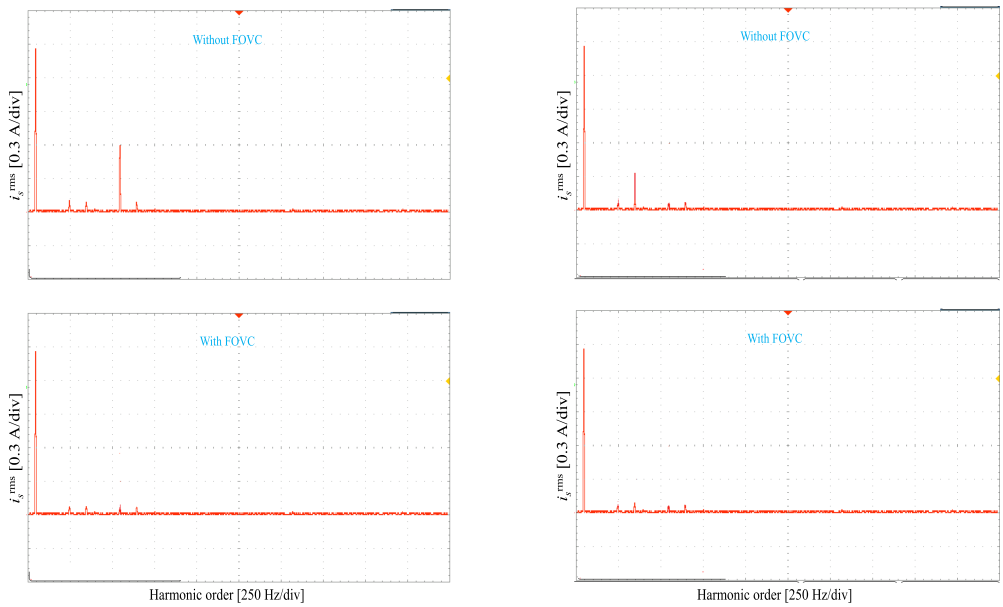

Fig. 17. Measured harmonic spectrum of the current injected into the grid. (a) $L_{ac} = 1.25$ mH. (b) $L_{ac} = 3.5$ mH.

the measured waveforms of the current injected into the grid for $L_{ac} = 3.5$ mH. As can be seen, the FOVC effectively damps the current oscillations despite the variations in the ac-side inductance.

Fig. 17 shows the measured harmonic spectrum of the current injected into the grid. It can be seen in Fig. 17(a) and (b) that the proposed FOVC effectively suppresses the current harmonics even with the variations in the CL-filter resonance.

VI. Conclusion

This article has presented the impedance-based analysis of an FOVC for active damping of multiparalleled grid-connected CSIs in which the filter capacitor voltage is fed back to the PWM current reference through a fractional-order derivative controller. A passivity approach further has been proposed to select the FOVC parameters considering the digital control delay. The proposed FOVC as a generalized virtual impedance adequately damps the CL-filter resonance and current oscillations even with variations in the grid impedance and the number of paralleled CSIs. Simulation and experimental results verify the efficacy of the proposed active damping technique.

References

[1] J. Rocabert, A. Luna, F. Blaabjerg, and P. Rodríguez, "Control of power converters in AC microgrids," *IEEE Trans. Power Electron.*, vol. 27, no. 11, pp. 4734–4749, Nov. 2012.

[2] A. A. A. Radwan and Y. A.-R. I. Mohamed, "Analysis and active suppression of AC- and DC-side instabilities in grid-connected current-source converter-based photovoltaic system," *IEEE Trans. Sustain. Energy*, vol. 4, no. 3, pp. 630–642, Jul. 2013.

[3] X. Wang, F. Blaabjerg, and P. C. Loh, "Virtual RC damping of LCL-filtered voltage source converters with extended selective harmonic compensation," *IEEE Trans. Power Electron.*, vol. 30, no. 9, pp. 4726–4737, Sep. 2015.

[4] X. Wang, Y. W. Li, F. Blaabjerg, and P. C. Loh, "Virtual-impedance-based control for voltage-source and current-source converters," *IEEE Trans. Power Electron.*, vol. 30, no. 12, pp. 7019–7037, Dec. 2015.

[5] T. Liu, J. Liu, Z. Liu, and Z. Liu, "A study of virtual resistor-based active damping alternatives for LCL resonance in grid-connected voltage source inverters," *IEEE Trans. Power Electron.*, vol. 35, no. 1, pp. 247–262, Jan. 2020.

[6] Z. Bai, H. Ma, D. Xu, B. Wu, Y. Fang, and Y. Yao, "Resonance damping and harmonic suppression for grid-connected current-source converter," *IEEE Trans. Ind. Electron.*, vol. 61, no. 7, pp. 3146–3154, Jul. 2014.

[7] Z. Miao, W. Yao, and Z. Lu, "Single-cycle-lag compensator-based active damping for digitally controlled LCL/LLCL-type grid-connected inverters," *IEEE Trans. Ind. Electron.*, vol. 67, no. 3, pp. 1980–1990, Mar. 2020.

[8] A. Aapro, T. Messo, T. Roinila, and T. Suntio, "Effect of active damping on output impedance of three-phase grid-connected converter," *IEEE Trans. Ind. Electron.*, vol. 64, no. 9, pp. 7532–7541, Sep. 2017.

[9] L. Jia, X. Ruan, W. Zhao, Z. Lin, and X. Wang, "An adaptive active damper for improving the stability of grid-connected inverters under weak grid," *IEEE Trans. Power Electron.*, vol. 33, no. 11, pp. 9561–9574, Nov. 2018.

[10] E. Rodriguez-Diaz, F. D. Freijedo, J. C. Vasquez, and J. M. Guerrero, "Analysis and comparison of notch filter and capacitor voltage feedforward active damping techniques for LCL grid-connected converters," *IEEE Trans. Power Electron.*, vol. 34, no. 4, pp. 3958–3972, Apr. 2019.

[11] J. Roldan-Perez, E. J. Bueno, R. Pena-Alzola, and A. Rodriguez-Cabero, "All-pass-filter-based active damping for VSCs with LCL filters connected to weak grids," *IEEE Trans. Power Electron.*, vol. 33, no. 11, pp. 9890–9901, Nov. 2018.

[12] R. Pena-Alzola, M. Liserre, F. Blaabjerg, R. Sebastian, J. Dannehl, and F. W. Fuchs, "Systematic design of the lead-lag network method for active damping in LCL-filter based three phase converters," *IEEE Trans. Ind. Informat.*, vol. 10, no. 1, pp. 43–52, Feb. 2014.

[13] M. A. Azghandi, S. M. Barakati, and A. Yazdani, "Impedance-based stability analysis and design of a fractional-order active damper for grid-connected current-source inverters," *IEEE Trans. Sustain. Energy*, vol. 12, no. 1, pp. 599–611, Jan. 2021.

[14] J. He, Y. W. Li, D. Bosnjak, and B. Harris, "Investigation and active damping of multiple resonances in a parallel-inverter-based microgrid," *IEEE Trans. Power Electron.*, vol. 28, no. 1, pp. 234–246, Jan. 2013.

[15] L. Hong, W. Shu, J. Wang, and R. Mian, "Harmonic resonance investigation of a multi-inverter grid-connected system using resonance modal analysis," *IEEE Trans. Power Del.*, vol. 34, no. 1, pp. 63–72, Feb. 2019.

[16] X. Wang, F. Blaabjerg, and P. C. Loh, "Passivity-based stability analysis and damping injection for multiparalleled VSCs with LCL filters," *IEEE Trans. Power Electron.*, vol. 32, no. 11, pp. 8922–8935, Nov. 2017.
[17] T. Chen, C.-K. Lee, and S. Y. R. Hui, "A general design procedure for multi-parallel modular grid-tied inverters system to prevent common and interactive instability," *IEEE Trans. Power Electron.*, vol. 34, no. 7, pp. 6025–6030, Jul. 2019.
[18] K. G. Khajeh, D. Solatialkaran, F. Zare, and N. Mithulananthan, "Harmonic analysis of multi-parallel grid- connected inverters in distribution networks: Emission and immunity issues in the frequency range of 0-150 kHz," *IEEE Access*, vol. 8, pp. 56379–56402, 2020.
[19] G. Tzounas, I. Dassios, M. A. A. Murad, and F. Milano, "Theory and implementation of fractional order controllers for power system applications," *IEEE Trans. Power Syst.*, vol. 35, no. 6, pp. 4622–4631, Nov. 2020.
[20] N. Mijat, D. Jurisic, and G. S. Moschytz, "Analog modeling of fractional-order elements: A classical circuit theory approach," *IEEE Access*, vol. 9, pp. 110309–110331, 2021.
[21] C. Xie, K. Li, J. Zou, and J. M. Guerrero, "Passivity-based stabilization of LCL-type grid-connected inverters via a general admittance model," *IEEE Trans. Power Electron.*, vol. 35, no. 6, pp. 6636–6648, Jun. 2020.
[22] L. Zhou *et al.*, "Inverter-current-feedback resonance-suppression method for LCL-type DG system to reduce resonance-frequency offset and grid-inductance effect," *IEEE Trans. Ind. Electron.*, vol. 65, no. 9, pp. 7036–7048, Sep. 2018.
[23] X. Wang and F. Blaabjerg, "Harmonic stability in power electronic-based power systems: Concept, modeling, and analysis," *IEEE Trans. Smart Grid*, vol. 10, no. 3, pp. 2858–2870, May 2019.
[24] H. Liu, L. Li, Y. Liu, D. Xu, and Q. Gao, "Passivity based damping design for grid-connected converter with improved stability," *IEEE Access*, vol. 7, pp. 185168–185178, 2019.
[25] Y. Jiang and B. Zhang, "Comparative study of Riemann-Liouville and Caputo derivative definitions in time-domain analysis of fractional-order capacitor," *IEEE Trans. Circuits Syst. II, Express Briefs*, vol. 67, no. 10, pp. 2184–2188, Oct. 2020.

M. Ali Azghandi received the M.Sc. degree from the Mazandaran University of Science and Technology, Babol, Iran, in 2013, and the Ph.D. degree from the University of Sistan and Baluchestan, Zahedan, Iran, in 2020, both in electrical engineering.

His research interests include modeling and control of power electronic converters, renewable electric power systems, and distributed electric power generation.

S. Masoud Barakati (Senior Member, IEEE) received the Ph.D. degree in electrical engineering from the University of Waterloo, Waterloo, ON, Canada, in 2008.

He is currently an Associate Professor with the University of Sistan and Baluchestan, Zahedan, Iran. He was an Associate Researcher with the University of Wisconsin–Madison, Madison, WI, USA, from 2008 to 2009. He was a Visiting Professor with Ryerson University, Toronto, ON, Canada, and Ecole Polytechnique de Montreal, Montreal, QC, Canada, in 2012 and 2014, respectively. His current research interests include power electronic circuits, control systems, renewable energy, flexible ac transmission system devices, matrix and multilevel converters, and mechatronic systems.

Dr. Barakati is the Editor-in-Chief for *International Journal of Industrial Electronics, Control and Optimization*.

Amirnaser Yazdani (Senior Member, IEEE) received the Ph.D. degree in electrical engineering from the University of Toronto, Toronto, ON, Canada, in 2005.

From 1995 to 2002, he was a Designer of track vacancy detection and other railway signaling systems with Maharan Engineering Corporation, Tehran, Iran. From 2005 to 2006, he was with Digital Predictive Systems, Inc., Mississauga, ON, Canada, and was involved in the design and manufacture of power converters for wind energy systems. From 2006 to 2011, he was an Assistant Professor with the University of Western Ontario, London, ON, Canada. He is currently a Professor with Ryerson University, Toronto, ON, Canada, and is involved in teaching and research in the general areas of power electronics and power systems. He has coauthored two books entitled *Voltage-Sourced Converters in Power Systems* (Hoboken, NJ, USA: Wiley/IEEE Press, 2010) and *Multi-Terminal Direct-Current Grids* (Hoboken, NJ, USA: Wiley/IEEE Press, 2014). His research interests include modeling and control of switching power converters, distributed electric power generation, microgrids, and control systems.

Dr. Yazdani is an Associate Editor for the IEEE TRANSACTIONS ON SMART GRID and IEEE TRANSACTIONS ON POWER ELECTRONICS. He is a Professional Engineer in the province of Ontario, Canada.